Available online at www.sciencedirect.com
SCIENCE DIRECT®
International Journal of Heat and Mass Transfer 48 (2005) 2219–2232
International Journal of HEAT and MASS TRANSFER
www.elsevier.com/locate/ijhmt

Heat, mass and momentum transport behaviors in directionally solidifying blade-like castings in different electromagnetic fields described using a continuum model

Daming Xu *, Yunfeng Bai, Hengzhi Fu, Jingjie Guo

School of Materials Science and Engineering, Harbin Institute of Technology, 92 West Da Zhi Street, P.O. Box 434, Harbin 150001, China

Received 26 December 2003; received in revised form 31 December 2004
Available online 3 March 2005

Abstract

A previous continuum model proposed and recently modified by the authors for describing the heat, mass and momentum transport phenomena in dendrite solidification process of alloy castings was further extended to the solidification cases in an arbitrary electromagnetic (EM)-fields. The extended continuum model and a FEM/FDM joint solution technique were successfully applied to the numerical simulations of directional solidification transport processes in blade-like castings of Pseudo-binary In718 base-4.85 wt.%Nb and Al–4.5 wt.%Cu alloys under a static or harmonic EM-field of different strengths/frequencies. The computational results demonstrate the availability of the present continuum modeling to treat an EM-STP problem, and also reveal that the volume-contraction-driven liquid feeding flow is much more difficult to be suppressed than the buoyancy-induced by means of applying a static magnetic field.

1. Introduction

Heat energy, species mass and momentum transfers are the basic and key transport phenomena occurring in solidification processes of various alloy castings. These transport processes will not only determine the solidification behaviors but also in turn exert important influences on the formations of various solidification defects, especially on all kinds of macro-segregation formations [1]. On the other hand, the solidification transport behaviors are closely related to the types and compositions of alloys, shapes and dimensions of the ingots/castings, and various external body-force fields that exert on the solidifying ingots/castings, such as the gravity, centrifugal forces and electromagnetic (EM) fields etc.

Lots of theoretical research efforts have been made on mathematical modeling for the transport phenomena of heat energy, species mass and momentum of liquid flow in the solidification processes of alloy ingots/castings using a continuum/mixture-averaging/one-phase [2–7] or multi-phase formulation technique [8–10]. Almost all these modeling and the corresponding computer simulations for the solidification cases were under the gravity field. The computational results demonstrate that the gravity (buoyancy force)-induced convections (i.e. thermal-/solutal-convections, or double-diffusion convections) can be an important influential aspect for the solidification transport behaviors and formations

* Corresponding author. Tel.: +86 451 86418624; fax: +86 451 86221048.
E-mail address: damingxu@hit.edu.cn (D. Xu).

0017-9310/$ - see front matter © 2005 Elsevier Ltd. All rights reserved.
doi:10.1016/j.ijheatmasstransfer.2004.12.020

Nomenclature

$\mathbf{A}_{2N}$	a basic geometric unit vector, $A_{2Nj} = [A_j \cdot F_j^{Nj}/(f_S^{1/2} \cdot L_j^d)]^2, j = 1,\ldots,5$, for the ($j$)th geometric component
$\mathbf{B}$	magnetic flux density vector
c_P	specific heat
C	concentration of solute mass
d_1, d_2	primary and secondary arm spacings of dendrite
D	diffusion coefficient of solute
$\mathbf{D}$	electric displacement vector
$\mathbf{E}$	electric field intensity vector
f	volume fraction
F	symbol for a function, or $\mathbf{F}$ for a force vector
$\mathbf{g}$	gravitational acceleration vector
h	latent heat of fusion
$\mathbf{H}$	magnetic field intensity vector
$\mathbf{J}$	electric current density vector
k	partition coefficient of solute
K	permeability coefficient
L	a length scale
P	pressure
q	heat flux density
R_f	solidification rate, $R_f = \partial f_S/\partial t$
t	time
t_f	local solidification time
T	temperature
$\mathbf{V}$	velocity vector, $\mathbf{V} = \mathbf{i} \cdot V_x + \mathbf{j} \cdot V_y + \mathbf{k} \cdot V_z$
x,y,z	3-D rectangular spatial coordinates
α	Fourier diffusion number, $\alpha = 4D_S t_f/(L_d)^2$
β	solidification shrinkage, $\beta = \rho_S/\rho_L - 1$
Δ	a increment symbol
ε	dielectric permittivity
η	dynamic viscosity
θ	a non-dimensional parameter representing the sensibility of the interdendritic liquid concentration-variation in response to the solid back diffusion (SBD), $\theta = (1+\beta) \cdot k \cdot f_S/f_L^2$
λ	thermal conductivity
μ	magnetic permeability
ρ	density
ρ_e	density of electric charge
φ	a non-dimensional micro-scale parameter representing the SBD extent with a general form of $\varphi = (D_S(T)/R_f)\boldsymbol{\zeta} \cdot \mathbf{A_{2N}}$, or a Fourier diffusion number with dendrite morphology modification [28]
Φ	a unified micro-scale parameter accounting for any finite SBD effects in dendrite solidification, $\Phi = \theta \cdot \varphi/(1 + \theta \cdot \varphi)$
∇	Hamiltonian operator, $\nabla = \mathbf{i} \cdot \partial/\partial x + \mathbf{j} \cdot \partial/\partial y + \mathbf{k} \cdot \partial/\partial z$ (in rectangular coordinates)
σ	electric conductivity
$\boldsymbol{\zeta}$	a normalized weighting vector for the basic geometric units, $\boldsymbol{\zeta} = \boldsymbol{\zeta}(\zeta_1, \zeta_2, \zeta_3, \zeta_4, \zeta_5)$

Subscripts

A	air
B	body force
C	cooling
d	dendrite
E	at the eutectic composition of an alloy
G	inducted by electromagnetic field
H	high temperature or heating
J	Joule heat
L	liquid phase or Lorentz force
Liq	liquidus
m	volume-averaged for the mixture of dendrites + interdendritic liquid phase (S + L)
M	shell mold
0	initial value or at a given condition
S	solid phase

Superscripts

i	a serial number denoting a time at which various variable fields are computed
*	at solid/liquid interface

of several kinds of macro-segregation [2,3,6,7]. Some of the computer modeling also account for the solidification-shrinkage (an inner force)-driven liquid flow (interdendritic feeding flow of liquid phase) [6,11,12], and thereby the specific macro-segregations caused, such as the positive macro-segregation (inverse segregations) in the surface regions adjacent to chill plates, or the negative macro-segregation formed in the places of sudden cross-section reductions [13,14].

In the past decades, a special materials processing technique, called electromagnetic processing of materials (EPM), has become more and more recognized as an important technology in advanced materials processing [15]. Some promising or in use EPM applications may include: using transverse or vertical static magnetic field to alleviate or control the natural convections in crystal growth processes [16–19] or penetration of pouring alloy melts deep into bulk liquid zones (electromagnetic brakes (EMBR)) in continuous casting (or DC casting) processes of various metallic ingots [20–22], applying various alternating EM-fields to DC casting processes for controls of melt meniscus shapes and the surface

qualities of the ingots [22–25], or grain refining of the solidified ingots through EM stirring/vibrating generations [26,27] etc. Therefore, it is of practical importance to perform modeling for the transport phenomena of heat energy, species mass and momentum of melt flow in various crystallizing materials or solidifying alloy ingots/castings which may be under various EM-fields.

A continuum model for describing heat, species mass and momentum transport phenomena in binary dendritic solidification processes, and the corresponding numerical methods with high solution efficiencies for the multi-fields-coupled solidification problems, were proposed by the present authors [5,6]. This model and numerical solution methods have been recently extended to a more general case of binary dendritic single-phase/eutectic solidification with any solid-back diffusion (SBD) of the solute and arbitrary dendrite morphologies [28]. The sample computations still show the feasibilities and efficiencies of the extended model and numerical solution methods [29]. The aim of this work is to further extend the continuum model to the binary dendrite solidification cases that are under static or alternating EM-fields. The computational tests with two kinds of alloys will be performed to demonstrate the solidification transport behaviors of heat energy, species mass and momentum of melt flow under different EM-fields, as well as the availability of the extended continuum model.

2. Model and computational procedures

The EM solidification transport phenomena to be modeled for an alloy shaped casting are assumed in a directional solidification process, which can be either in a transverse static magnetic field or in a harmonic EM-field. The shaped casting is 112 mm high and blade-like which has a neck of 28 mm wide and has bottom and top blocks of 56×38 mm and 56×32 mm, respectively. The adopted directional solidification configuration is similar to that in Refs. [14,29,30] except for that an EM-field is applied. The downwards withdrawal velocity for the assembly of the casting, CaO shell-mold and bottom copper cooler is assumed to be constant at $V_0 = 0.15$ mm/s. Due to the symmetry of the EM directional solidification system, one half of the system is chosen as the computational domain for the solidification transport processes. Fig. 1 shows the configuration and dimensions of the calculated directional solidification system for an alloy shaped casting in a transverse static magnetic field (right half). The temperature distributions in the heating zone and the cooling zone are assumed to be uniform at T_H and T_C, respectively. The configuration for the EM-directional-solidification case under a harmonic EM-field is similar to that of Fig. 1, and will be described in details in a later section of the paper.

The model for the solidification transport phenomena/processes (STP) of heat energy, species mass and momentum of liquid flow in a solidifying alloy casting/ingot under any an EM-field is extended from an author's previously proposed continuum model [29] based on the theory of Thermo-Magneto Hydro Dynamics [31]. The model has the formulation form of Eqs. (1)–(12) with the following assumptions:

(1) the external forces exerted on the solidifying system are only gravity and Lorentz force;
(2) no pores will occur, i.e. the geometric continuity, $f_L + f_S = 1$, holds for any region in the casting/ingot domain;
(3) the solidified dendrite phase is rigid and macroscopically static relative to the y–o–z coordinates, i.e. $\mathbf{V}_S \equiv 0$;
(4) local thermodynamic equilibrium holds at the microscopic solid-liquid interfaces;
(5) Newtonian and laminar liquid flow presents; and
(6) The model alloy is a binary system, or can be simplified to a pseudo-binary system.

Solidification heat energy transfer

$$(\rho c_P)_m \partial T/\partial t + \nabla(f_L \rho_L c_{PL} \mathbf{V}_L T) = \nabla(\lambda_m \nabla T) + \rho_S h(\partial f_S/\partial t) + q_J \quad (1)$$

where the electromagnetically inducted Joule heat

$$q_J = \mathbf{J}_G \cdot \mathbf{E} = \mathbf{J}_G^2/\sigma \quad (2)$$

Solidification species mass transfer

$$\partial(\rho C)_m/\partial t + \nabla(f_L \rho_L \mathbf{V}_L C_L) = \nabla[D_L \nabla(f_L \rho_L C_L) + D_S \nabla(f_S \rho_S C_S)] \quad (3)$$

Liquid–solid phase-change characteristic function for a specific binary alloy

$$T_{Liq} = F(C_L^*) \quad (4)$$

Solidification mass conservation

$$\partial \rho_m/\partial t = -\nabla(f_L \rho_L \mathbf{V}_L) \quad (5)$$

Momentum transfer for bulk/interdendritic liquid flow

$$\partial(f_L \rho_L \mathbf{V}_L)/\partial t + \nabla[(f_L \rho_L \mathbf{V}_L)\mathbf{V}_L] = \nabla[\eta \nabla(f_L \mathbf{V}_L)] - \nabla(f_L P_L) - (\eta f_L^2/K)\mathbf{V}_L + \mathbf{F}_B \quad (6)$$

For a general dendrite solidification case with any incomplete SBD, the time-differential mixture-averaged composition (TDMAC) term (a macro-scale variable) in the macroscopic solidification species mass transport Eq. (3) is closely related to the solute redistribution behaviors on the micro-scale of dendrites, and can be expressed into the following fully differential TDMAC form

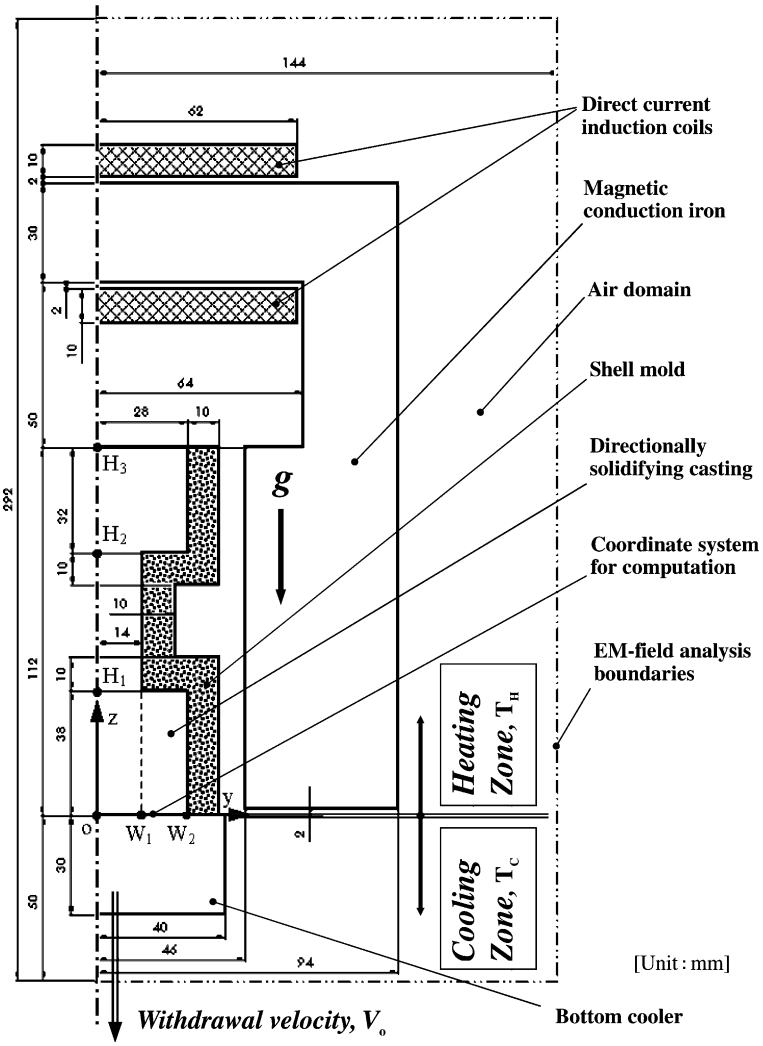

Fig. 1. Configuration and dimensions of the directional solidification of alloy shaped castings in a transverse static magnetic field (right half).

$$\partial(\rho C)_{\mathrm{m}}/\partial t = (\rho_{\mathrm{S}}C_{\mathrm{S}})^{*}\partial f_{\mathrm{S}}/\partial t + \Phi f_{\mathrm{S}}\partial(\rho_{\mathrm{S}}C_{\mathrm{S}})^{*}/\partial t + (\rho_{\mathrm{L}}C_{\mathrm{L}})\partial f_{\mathrm{L}}/\partial t + f_{\mathrm{L}}\partial(\rho_{\mathrm{L}}C_{\mathrm{L}})/\partial t \quad (7)$$

where, the unified microscale-parameter Φ, accounting for any finite SBD effects in the solidifying dendrite phases, has been found to be a function of other two non-dimensional parameters of interdendritic liquid-concentration-variation in response to the SBD (or SBD end effects of dendrite solidification), $\theta = (1+\beta)kf_{\mathrm{S}}/f_{\mathrm{L}}^2$, and Fourier diffusion number with dendrite-morphology modification, $\varphi = (D_{\mathrm{S}}(T)/R_f)\boldsymbol{\zeta}\cdot\mathbf{A}_{2N}$ [28]. The function for the non-dimensional parameter of finite dendritic SBD effects, Φ, can be approximately expressed as

$$\Phi = \theta\varphi/(1+\theta\varphi) \quad (8)$$

Correspondingly, in the mixture-average-based equation for the dendritic solidification mass conservation, i.e. Eq. (5), the time-differential mixture-averaged density (TDMAD) term (also a macro-scale variable) can be approximately expressed as [29]

$$\partial\rho_{\mathrm{m}}/\partial t \approx \rho_{\mathrm{S}}^{*}\partial f_{\mathrm{S}}/\partial t + \Phi f_{\mathrm{S}}\partial\rho_{\mathrm{S}}^{*}/\partial t + \rho_{\mathrm{L}}\partial f_{\mathrm{L}}/\partial t + f_{\mathrm{L}}\partial\rho_{\mathrm{L}}/\partial t \quad (9)$$

Using the true temperature-/composition- and phase-state-dependent densities for both the liquid and solid phases of the solidifying alloy, the TDMAD term of Eq. (5), expressed by Eq. (9), can fully account for the volume-changes of the alloy melt in both bulk-liquid region and mushy (S + L) region (during solidification volume-contractions usually occurring). The volume-

contraction can be induced both by the phase-change (e.g. the case of solidification shrinkage), and by the variations in both the temperature and concentrations (thermal/solutal expansions). With a proper numerical solution procedure, such as the methods proposed in Ref. [6], the strong P_L couplings for the buoyancy- and solidification shrinkage-induced melt flow can be fully and efficiently solved.

In the present momentum transfer equation, Eq. (6), the pressure gradient term contains two parts for the liquid flow in mushy zone (interdendritic liquid flow), i.e.

$$\nabla(f_L P_L) = f_L \nabla P_L + P_L \nabla f_L \tag{10}$$

The second term on the right-hand side of Eq. (10) represents a force to compress or distend the flowing interdendritic liquid-phase, causing its actual velocity to change in the direction of $-\nabla f_L$. Furthermore, this compressing/distending force is provided by the surrounding solid-phase (a stationary dendrites array in the present solidification case), can not be balanced by the flowing liquid-phase itself, therefore, should be viewed as an external force to the liquid-phase. The body force term, induced by external fields, in Eq. (6) for the bulk/interdendritic liquid flow includes the gravity and Lorentz force, $\mathbf{F}_L$:

$$\mathbf{F}_B = f_L \rho_L \mathbf{g} + \mathbf{F}_L \tag{11}$$

where, the Lorentz force acting on the flowing liquid-phase during solidification can be further expressed as:

$$\begin{aligned}\mathbf{F}_L &= \sigma f_L(\mathbf{E} + \mathbf{V}_L \times \mathbf{B}) \times \mathbf{B} \\ &= f_L\{\mathbf{J}_G \times \mathbf{B} + \sigma[(\mathbf{V}_L \cdot \mathbf{B})\mathbf{B} - \mathbf{B}^2\mathbf{V}_L]\}\end{aligned} \tag{12}$$

For the influences of EM-fields on the solidification transport behaviors, the extended continuum model of Eqs. (1)–(12) shows that the time- and position-dependent fields of magnetic flux density $\mathbf{B}$ and electromagnetically inducted current $\mathbf{J}_G$ in the modeled alloy casting/ingot domain need to be simultaneously determined. Maxwell's equations and the corresponding constitutive relationships for all the involved materials in the present EM-solidification systems, including the casting alloys, shell-mold and bottom cooler and the environmental air etc, provide such modeling equations, which can be expressed by [31]:

Maxwell's equations

$$\nabla \times \mathbf{H} = \mathbf{J} + \partial \mathbf{D}/\partial t \quad (\text{law of Maxwell} - \text{Ampere}) \tag{13}$$

$$\nabla \times \mathbf{E} = -\partial \mathbf{B}/\partial t \quad (\text{EM} - \text{induction law of Faraday}) \tag{14}$$

$$\nabla \cdot \mathbf{D} = \rho_e \quad (\text{law of Gauss}) \tag{15}$$

$$\nabla \cdot \mathbf{B} = 0 \quad (\text{continuity of magnetic flux}) \tag{16}$$

Constitutive equations for the involved EM-medium materials

$$\mathbf{D} = \varepsilon \mathbf{E} \quad (\text{constitutive relationship of electric properties}) \tag{17}$$

$$\mathbf{B} = \mu \mathbf{H} \quad (\text{constitutive relationship of magnetic properties}) \tag{18}$$

$$\mathbf{J} = \sigma(\mathbf{E} + f_L \mathbf{V}_L \times \mathbf{B}) \quad (\text{Ohm law for the moving metallic melt}) \tag{19}$$

Besides the solidifying castings, Eq. (19) is also available for other EM-mediums where no phase-change occurs and $\mathbf{V}_L = 0$ or/and $\sigma = 0$. Different EM-medium materials will cause the EM-fields within them to act differently via their EM-properties of electric conductivity, magnetic permeability and dielectric permittivity. This is also true in the solidifying alloy metals, because the EM-related properties of the alloys in liquid and solid states usually are different besides varying with the temperature and compositions. These variations in the properties with the phase-states/temperature/compositions, however, are not significant (usually within an order of magnitude), therefore constant and equal EM-related properties data are used for the same alloy castings in the present computations for simplicity. Constant EM-properties are also taken for other corresponding EM-mediums, i.e. the CaO shell-mold and bottom copper cooler etc.

There are seven independent variables involved in the extended continuum model of Eqs. (1)–(19) for describing the EM-STP behaviors in a binary solidification process. All these variable fields are coupled one to each others, among which the dominant couplings include the nonlinear and strong correlations of solidification T–f_S–C_L and P_L–$\mathbf{V}_L$. The necessity to add a liquid–solid (L–S) phase-change function, Eq. (4), into the STP-based model comes from: The first is to close the mathematic model, which serves as an implicit restriction to determine a given temperature- and concentration-linked phase-field changing (mixture-averaged or macro-scale $f_S(t,x,y,z)$) problem [32], similar to the role of the solidification mass-continuity Eq. (5), in a sense mathematically, for solving a strong P_L–$\mathbf{V}_L$ coupling problem; the second is to specify the L–S phase-change characteristic for a given alloy system, i.e. to characterize the nonlinear and strong coupling behavior of T–f_S–C_L in a specific alloy solidification process [5,33]. Therefore, Eq. (4) should be an indispensable part to a complete STP-model.

In the present computer modeling based on Eqs. (1)–(19), the coupled fields of temperature, solid volume-fraction, concentration, pressure and flow velocity of the alloy melt are calculated in a finite-differential control-volume scheme using the numerical solution

methodologies proposed by the present authors. The strongly coupled T–f_S–C_L fields are solved by the simultaneously numerical solution procedure that is previously proposed in Ref. [5] and recently modified for a general binary solidification case of any incomplete SBD effects and arbitrary dendrite morphologies [33,28,29]. The nonlinearly and tightly linked P_L–$\mathbf{V}_L$ fields for both the bulk and interdendritic liquid phase are numerically solved using a direct-SIMPLE scheme proposed by the authors [6] and further extended to accommodate the Lorentz force [34].

The boundary conditions of the STP-related governing Eqs. (1)–(12) for a blade-like casting with the configuration shown in Fig. 1 can be written as

$$\begin{aligned}&(1)\ \text{at } z=0 \quad \text{and} \quad y\in[0,W_2]:\\ &\partial T/\partial z=(\lambda_A/L_{A1})(T-T_{Cooler}),\\ &\partial C/\partial z=0,\ V_y=0 \text{ and } V_z=0\end{aligned} \tag{20}$$

$$\begin{aligned}&(2)\ \text{at } z=H_1 \quad \text{and} \quad y\in[W_1,W_2]:\\ &\partial T/\partial z=(\lambda_A/L_{A3})(T-T_M),\\ &\partial C/\partial z=0,\ V_y=0 \text{ and } V_z=0\end{aligned} \tag{21}$$

$$\begin{aligned}&(3)\ \text{at } z=H_2 \quad \text{and} \quad y\in[W_1,W_2]:\\ &\partial T/\partial z=(\lambda_A/L_{A5})(T-T_M),\\ &\partial C/\partial z=0,\ V_y=0 \text{ and } V_z=0\end{aligned} \tag{22}$$

$$\begin{aligned}&(4)\ \text{at } z=H_3 \quad \text{and} \quad y\in[0,W_2]:\\ &\partial T/\partial z=q_{Conve.}+q_{Radia.},\ \partial C/\partial z=0,\\ &P_L=0,\ \partial V_y/\partial z=0 \text{ and } V_z=V_{fd}\end{aligned} \tag{23}$$

$$\begin{aligned}&(5)\ \text{at } y=0 \quad \text{and} \quad z\in[0,H_3]:\partial T/\partial y=0,\\ &\partial C/\partial y=0,\ V_y=0 \text{ and } \partial V_z/\partial y=0\end{aligned} \tag{24}$$

$$\begin{aligned}&(6)\ \text{at } y=W_2 \quad \text{and} \quad z\in[0,H_1]:\\ &\partial T/\partial y=(\lambda_A/L_{A2})(T-T_M),\\ &\partial C/\partial y=0,\ V_y=0 \text{ and } V_z=0\end{aligned} \tag{25}$$

$$\begin{aligned}&(7)\ \text{at } y=W_1 \quad \text{and} \quad z\in[H_1,H_2]:\\ &\partial T/\partial y=(\lambda_A/L_{A4})(T-T_M),\\ &\partial C/\partial y=0,\ V_y=0 \text{ and } V_z=0\end{aligned} \tag{26}$$

$$\begin{aligned}&(8)\ \text{at } y=W_2 \quad \text{and} \quad z\in[H_2,H_3]:\\ &\partial T/\partial y=(\lambda_A/L_{A6})(T-T_M),\\ &\partial C/\partial y=0,\ V_y=0 \text{ and } V_z=0\end{aligned} \tag{27}$$

where, the air gap thicknesses, L_{Ai}, $i=1,2,\ldots,6$, take constant values between 0.05 and 0.15 mm, in the present modeling; the top feeding rate, $V_{fd}=\{(\Sigma\Delta W_{j,k})^{i+1}/[\Delta t^{i+1}\cdot(\Sigma f_{Lj,K_0}A_j)^{i+1/2}]$ (for $f_{Lj,K_0}>f_{Lc}$); 0. (for $f_{Lj,K_0}\leqslant f_{Lc}$)}, where, $(\Sigma\Delta W_{j,k})^{i+1}$ and $(\Sigma f_{Lj,K_0}A_j)^{i+1/2}$ represent the total liquid-volume contraction over the casting domain in a time interval Δt^{i+1} and the effective liquid area on the casting top at the time $t^{i+1/2}$, respectively. In the present modeling, the critical liquid-volume fraction that allows a free top feeding takes, $f_{Lc}=0.35$.

Under the assumptions of small and negligible variations in the free-surface shape of the metallic melt in the EM-solidification processes and constant EM-properties of the solidifying materials, the couplings between the EM-fields and the STP-related fields can be simplified as one-way influences. In this case, the solidification transport processes will not exert evident influences on the EM-fields, therefore, in the model numerical solution processes the computations for the EM-fields of the solidification system can be prior to that of the STP calculations at each time step. In this way, entire numerical computations for a full model solution to Eqs. (1)–(27) can be significantly simplified. In the present numerical modeling, the computations of the EM-fields, which are on the basis of Eqs. (13)–(19), are performed using an available commercial software, ANSYS 6.1 (*ANSYS is a trademark of ANSYS, Inc., Pittsburgh, USA), for all the EM-solidification samples below.

In ANSYS EM-field computations for a given EM-solidification system, several types of EM-boundary conditions are available to choose depending on the natures of the EM-boundaries of the system to treat. Take the whole directional solidification system with a transverse static magnetic field applied as example (shown by Fig. 1 as a half-part), all the "FM-field analysis boundaries" (the symmetrical axis and the dot-dot-dashed lines) are set as "parallel". The EM-boundaries for the sample computations with alternating EM-fields in Section 4 also involve some "far-field boundaries". Fig. 3 of Ref. [35] illustrates a such harmonic EM-solidification system with a "infinite-equivalent boundary", which is adopted for the sample computations in Section 4.

In the ANSYS EM-calculations, some FEM schemes are adopted, while the numerical solution methods used for the EM-STP computations are FDM-based [5,6,33,34]. To joint these two different numerical schemes, special mathematical treatment techniques and computer codes were developed [35] to convert the FEM-analyzed EM-results, output from ANSYS 6.1, to the FDM-formatted data files that are available for the FDM-based EM-STP simulation program of the authors.

All the numerical simulations are performed on PC-computers. The mesh pattern for the half blade-like casting and one side of shell-mold, shown in Fig. 1, and the numbers of finite differential control volumes made in the casting and mold domains are all same as those used in Ref. [29] (i.e. 1680 and 936 mesh elements for the half casting and one side of the shell-mold, respectively). A STP-computation example for an entire EM-directional solidification process of alloy shaped casting will take

about 7–10 s of CPU-time on average for one second of the real directional-solidification-time on a PC-computer of 2.4 GHz CPU clock frequency, depending on the types of the alloys and the EM-fields applied etc.

3. Solidification in transverse static magnetic fields

The configuration and dimensions of the directional solidification of alloy shaped castings in a transverse static magnetic field has been shown in Fig. 1. In the illustration the blade-like casting is at its initial position for the directional solidification. The transverse stationary magnetic field in the shaped casting was simulated in a FEM-meshing pattern for this initial layout using ANSYS 6.1. The FEM-analyzed results indicate that the strength and direction distributions of the generated transverse static magnetic vectors are nearly uniform and perpendicular to the symmetrical axis of the system [36]. It is further assumed that during the directional solidification processes, the applied transverse static magnetic field in the casting keeps unchanged, for simplicity. Pseudo-binary In718 base-4.85 wt.%Nb system [37] is adopted as model alloy for the calculation samples of this section. The used EM-STP properties for the assumed Pseudo-binary In718 system are listed in Table 1 [37,38]. In the adopted properties, the permeability function $K(f_L)$ is assumed to be the same basically as that used in a STP-simulation for steel ingots [39], with a modification for a very beginning stage of dendrite solidification in order to meet the zero Darcian-resistance requirement of a continuum momentum transfer model.

The initially uniform temperatures for the alloy melt in casting domain and for the shell mold are set at $T_0 = 1450$ °C and $T_{M0} = 1500$ °C, respectively. The initial conditions (at $t = 0$ s) of the velocity and concentration for the casting alloy melt are assumed to be uniform and taken as $\mathbf{V}_L = 0$ and $C_{L0} = [\rho_S(T_C, C_0)/\rho_L(T_0, C_{L0})]C_0$, where $C_0 = 4.85$ wt.%Nb, respectively. The temperatures of heating and cooling chambers and for the bottom cooler are assumed to be uniform and constant at $T_H \equiv 1600$ °C, $T_C \equiv 45$ °C and $T_{Cooler} \equiv 45$ °C, respectively, for the entire directional solidification processes (i.e. for $t \geqslant 0$ s).

Fig. 2 shows comparisons for the velocity vectors of liquid flow and relative pressure/temperature distributions in directionally solidified In718 shaped castings at $t = 21.0$ s in the transverse stationary magnetic fields of different strengths: 0, 500, 1000, 2500 and 10 kAmpere-turns (At), respectively. It can be seen that with increase of the static magnetic strength, the electromagnetic breaking (EMBR) effects on the liquid flow [15,17–22] increase significantly. Under zero-magnetic condition (i.e. only under gravity) at this directional cooling/solidification stage, an obvious natural convection of the maximum velocity, $V_{L^{max}} = 1.896$ mm/s, occurs in the bulk liquid region. This convection is

Table 1
The EM-STP properties for the pseudo-binary In718 base-4.85 wt.%Nb system used in the present work [37,38]

$\lambda_S(T) = 6.4268 \times 10^{-3} + 1.7614 \times 10^{-5}\, T$ (T in [K])	[W/mm K]
$\lambda_L(T, C_L) = 3.005 \times 10^{-2}$ (T in [K])	[W/mm K]
$c_{PS}(T) = \begin{cases} 0.34593 + 2.9483 \times 10^{-4} T & (T \leqslant 437\ \text{K}) \\ 0.39405 + 1.8468 \times 10^{-4} T & (437\ \text{K} < T \leqslant 928\text{K}) \\ -0.13404 + 7.5405 \times 10^{-4} T & (928\ \text{K} < T \leqslant 1668\ \text{K}) \end{cases}$	[J/g K]
$c_{PL}(T, C_L) = 1.1$	[J/g K]
$\rho_S(T, C_L) = 7.6205 \times 10^{-3}$	[g/mm^3]
$\rho_L(T, C_L) = 6.95 \times 10^{-3} - 1.5 \times 10^{-7}\,(T - T_{Liq}) + 9.27 \times 10^{-6}\,(C_L - C_O)$	[g/mm^3]
$h(C_S) = 295$	[J/g]
$T_{Liq}(C_{L/Nb}) = 1345.4318 - 3.55786086 \times 10^{(0.0873 \cdot CL/Nb)}$ ($C_{L/Nb} \in$ [4.8,19.1 wt.%Nb])	[°C]
$T_E = 1180$	[°C]
$C_E = 19.1$	[wt.%Nb]
$k(C_{L/Nb}) = 0.993 - 0.118\ C_{L/Nb} + 0.0046\ (C_{L/Nb})^2$ ($C_{L/Nb}$ in [wt.%Nb])	[–]
$D_{L/Nb\ In718}\ (T\ °C) = 3 \times 10^{-3}$	[mm^2/s]
$D_{S/Nb\ In718}\ (T\ °C) = 560 \exp[-33676/(T + 273.15)]$	[mm^2/s]
$\eta(T) = 1.79 \times 10^{-4} \exp[6038/(T + 273.15)]$, $T \in [1350, 1475\ °C]$	[Pa s] (=[N · s/m^2] = [g/mm · s])
$K = \begin{cases} 4.0 \times 10^{-4} f_L^{3.0} & (f_L \leqslant 0.7088) \\ 1.6318 f_L^{27.155} & (0.7088 < f_L \leqslant 0.99999) \\ 1.0 \times 10^{18} & (f_L > 0.99999) \end{cases}$	[mm^2]
$d_1 = 12.8(\partial T/\partial t)^{-1.138}$ ($\partial T/\partial t$ in [°C/s])	[mm]
$d_2 = 8.998 \times 10^{-3} t_f^{0.5}$ (t_f in [s])	[mm]
$\sigma = 734.214$	[S/mm]

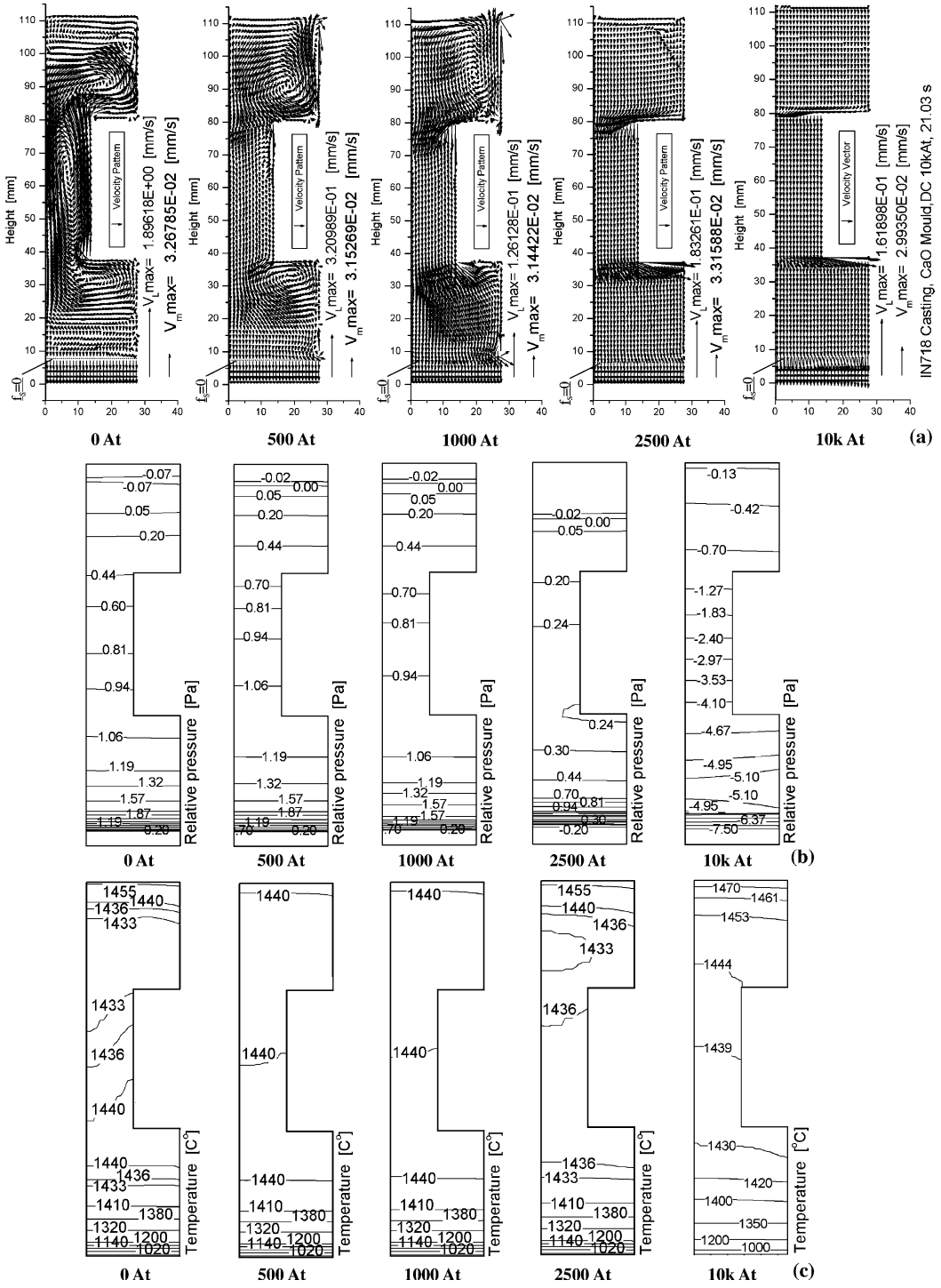

Fig. 2. Influences of transverse static magnetic strengths on the liquid flow behaviors and relative pressure/temperature distributions in directionally solidified In718 shaped castings at $t = 21.0$ s: (a) velocity vectors of liquid phases; (b) contours of relative pressure; (c) contours of temperature.

primarily driven by the vertical and lateral temperature gradients in the shaped casting, see Fig. 2(c)-0 At (the Nb solute has a higher density than the base alloy melt). When a horizontal static magnetic field of 500 At is

applied, the natural convection is weakened to a level of $V_{L^{max}} = 0.321$ mm/s, though its flow pattern is similar to that of zero-magnetic field to some extent. When the magnetic strength further enhances from 500 to 2500 At, it can be seen that the buoyancy-induced convection is almost suppressed (the $V_{L^{max}}$ for the 2500 At case is decreased by one order of magnitude compared to that with zero-magnetic field). Under the even stronger magnetic field of 10 kAt, it can be seen that the bulk liquid flow pattern approaches to a type of pure volume-contraction-feeding.

However, from Fig. 2(a) it is interesting to note that, although the gravity-induced convection can be significantly weakened when the strength of the applied transverse magnetic field enhances to 10 kAt, the magnitudes of the interdendritic feeding flow remains almost unchanged (see each $V_{m^{max}}$ value). This phenomenon indicates that the thermal/solutal contraction and solidification-shrinkage, acting as an inner force, have a much stronger ability to drive the liquid phase to flow (including to penetrate through the dendritic networks) than that by a buoyancy [6].These results are enforced by the solidification mass continuity, Eq. (5), and the "no-pore-occurring" requirement, Assumption (2). Therefore, the volume-contraction-driven liquid flow appears to be much more difficult to be suppressed by a transverse static magnetic field than the buoyancy-driven natural convections.

Fig. 2(b) shows comparisons of the relative pressure distributions corresponding to the each liquid flowing behavior under the transverse static magnetic fields of different strengths, shown in Fig. 2(a). It can be seen that, due to the relatively weak convection (the $V_{L^{max}} < 2$ mm/s), the isobars under all the static magnetic conditions are approximately flat. Furthermore, with the liquid flow weakened by the increasing static magnetic strength (therefore with less and less disturbances from the weakening flow momentums), the relative pressure distribution progressively approaches to an approximate static-pressure type, see the case of 10 kAt in Fig. 2(b).

The temperature contours in the directionally solidifying shaped castings corresponding to the each magnetic strength case of Fig. 2(a) are shown in Fig. 2(c). Comparison among these temperature distributions shows that, with the weakened natural convections due to the increase of magnetic strength, the longitudinal temperature gradients in the solidifying castings keep increasing and approaches to a pure-conduction type for the directional solidification heat transfers, see the cases of 0 At and 10 kAt of Fig. 2(c).

The influences of the different lateral static-magnetic strengths on the final macro-composition distribution in solidified In718 blade-like casting may be shown by Fig. 3, which is in a final solidification stage. First, it can be seen that, under the present directional solidification condition, the In718 blade-like casting is subject to channel-type segregation formations [1]. From Fig. 3 it also can be seen that, with the liquid-phase convection being progressively weakened, the channel-segregation becomes severer and severer. This result implies that the downwards liquid flow may promote the vertically

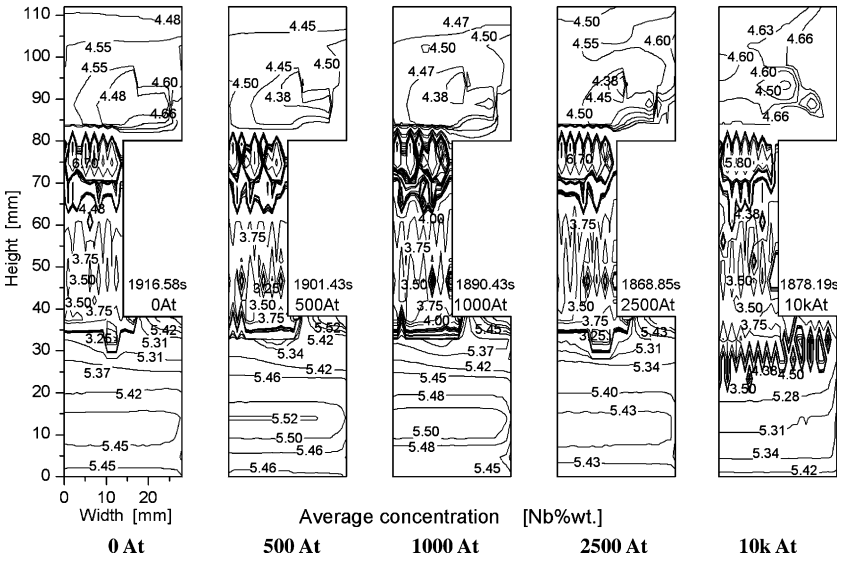

Fig. 3. Influences of the different transverse static magnetic strengths on the macro-composition distribution in the directionally solidified In718 shaped castings at a later stage and on the freezing time to arrive at the same solidification stage. (Under the same solidification condition as that of Fig. 2.)

parallel channel-segregation to form, while a convective circulation can help to homogenize the local (micro-scale) solute distribution.

4. Solidification under alternating electromagnetic fields

For this group of EM-STP sample computations, a nearly vertical harmonic-EM-field is induced by a 5-turn coil, through which alternating currents of different Ampere-turns and different frequencies pass. Under these EM-directional solidification cases, the shaped castings can be partially heated by the EM-induction coils that are assumed to be fixed to the directional furnace, besides being heated in the heating chamber of temperature T_H. In such an EM-directional-solidification configuration, the shaped castings will move out away from the EM-coils at the velocity of V_0 with the solidification proceeding, therefore, the EM-field distributions induced in the directional solidifying castings will change greatly. To account for such highly varying EM-fields in the downwards-withdrawn shaped castings, a technique of subsection interpolation is adopted.

For the present modeling, the heights of shaped castings are divided into 12 subsections of 10 mm high, and the vector distributions of induced magnetic flux densities and inducted currents at these 13 boundary positions of the divided subsections are calculated by ANSYS 6.1, and converted to the FDM-based data files [35] that are available for the subsequent STP-computations by the authors' simulation program. Interpolation method is used to determine the induced fields of magnetic flux densities and inducted currents at any solidification stage (at a t^{i+1} time's withdrawal distances). Fig. 4 illustrates the configurations and positions of a directionally solidifying shaped casting relative to the induction coils at the 12 different solidification stages under a harmonic EM-field.

Al–4.5 wt.%Cu alloy system is used as the model alloy for the sample computations of this section. The properties of the Al–4.5 wt.%Cu system for the present EM-STP simulation are same as those used in Ref. [29]. For Al–4.5 wt.%Cu system, the initial melt and mold temperature are set at the same temperature of 700 °C, and the temperature in the heating and cooling chambers and of the bottom cooler are again assumed to be uniform and constant at 950, 25 and 25 °C, respectively, for the entire EM-directional solidification process. The initial conditions for other fields are similar to that for the sample computation of Section 3, i.e. $\mathbf{V}_L = 0$ and $C_{L0} = [\rho_S(T_C, C_0)/\rho_L(T_0, C_{L0})]C_0$ at $t = 0$ s.

It is very known that the harmonic EM-fields of different frequencies will exert highly different influences on the transport behaviors in the processed metallic materials/melts through the Joule heating and Lorentz forces (skin effects). To show the availability of the present modeling for such responses of the STP in directionally

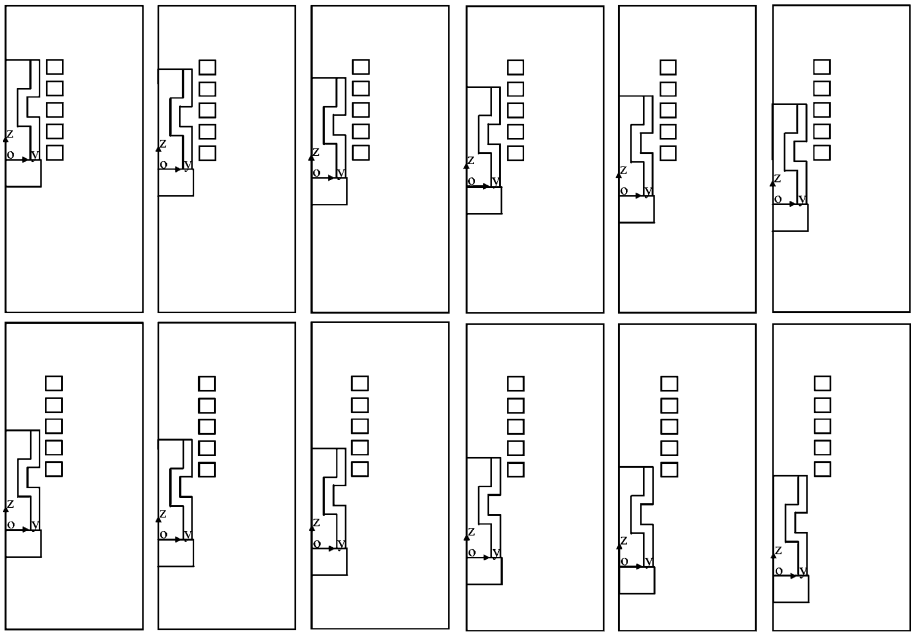

Fig. 4. Configurations and positions of a shaped casting relative to the induction coils at 12 different stages of directional solidification under harmonic EM-fields. At each position shown, FEM-based EM-field computations were made for interpolations of the EM-fields for the FDM-based STP-simulation at any withdrawal distance of the directionally solidifying alloy casting.

solidifying alloy shaped castings to the frequencies of the applied harmonic EM-fields, Fig. 5 gives a comparison of the calculated solidification transport-behaviors of Al–4.5 wt.%Cu castings under a harmonic EM-fields of the same current load of 2500 At but with different frequencies, at a withdrawal/cooling time of 10.01 s. It can be seen that for the same alloy casting and at the same withdrawal/cooling time, the distributions of the resulting Lorentz force vectors and its y-/z-components and the inducted Joule heats for the EM-frequencies of 50, 1000 and 20 kHz vary significantly. The general tendency of the variations in these field distributions is that, with the frequency increasing the EM-field penetration depth into the metallic casting decreases, so do the strong Lorentz forces and Joule heating effects, see Fig. 5(a)–(d). These calculated results may well demonstrate the feasibility of the present continuum modeling to account for such EM skin-effects, which are caused by the interaction between an alternating EM-field and metallic work-piece [23,24].

Under the actions of harmonic EM-fields with the different skin effects, the STP-behaviors in the solidifying shaped castings in the same EM-directional solidification configuration system are shown in Fig. 5(e) through Fig. 5(h). From Fig. 5(e) it can be seen that under the 50 Hz EM-field, the EM-driven very strong convections (the $V_{L^{max}} > 280$ mm/s) occupy the entire bulk liquid region, and leads to several negative pressure holes forming in the bulk liquid region, see Fig. 5(f)-50 Hz. While when the EM-frequency increases to 1000 Hz and further to 20 kHz, on one hand, the $V_{L^{max}}$ decreases to 205 and 65 mm/s, respectively, on the other hand, the relatively strong liquid circulations appear tending to close to the surface area of the lower casting block, see Fig. 5(e). Fig. 5(g) and (h) show the corresponding distributions of temperature and solid volume-fraction. It

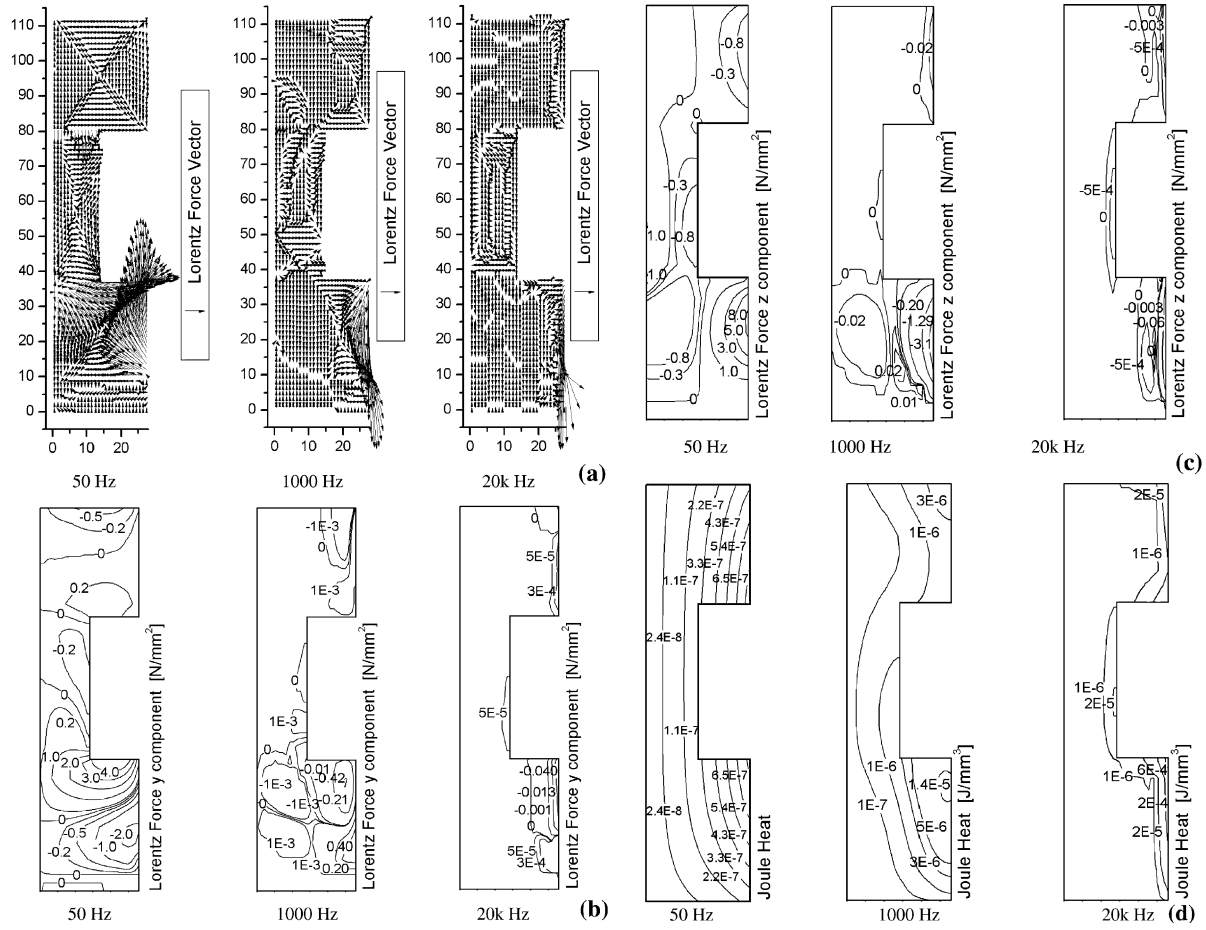

Fig. 5. Comparison of the directional solidification transport behaviors of Al–4.5 wt.%Cu shaped casting under harmonic magnetic fields (2500 At) of different frequencies at $t = 10.01$ s: (a) Lorentz force vectors; (b) y-component of the Lorentz force; (c) z-component of the Lorentz force; (d) contours of Joule heat; (e) velocity vectors; (f) contours of relative pressure; (g) contours of temperature; (h) contours of solid volume fraction.

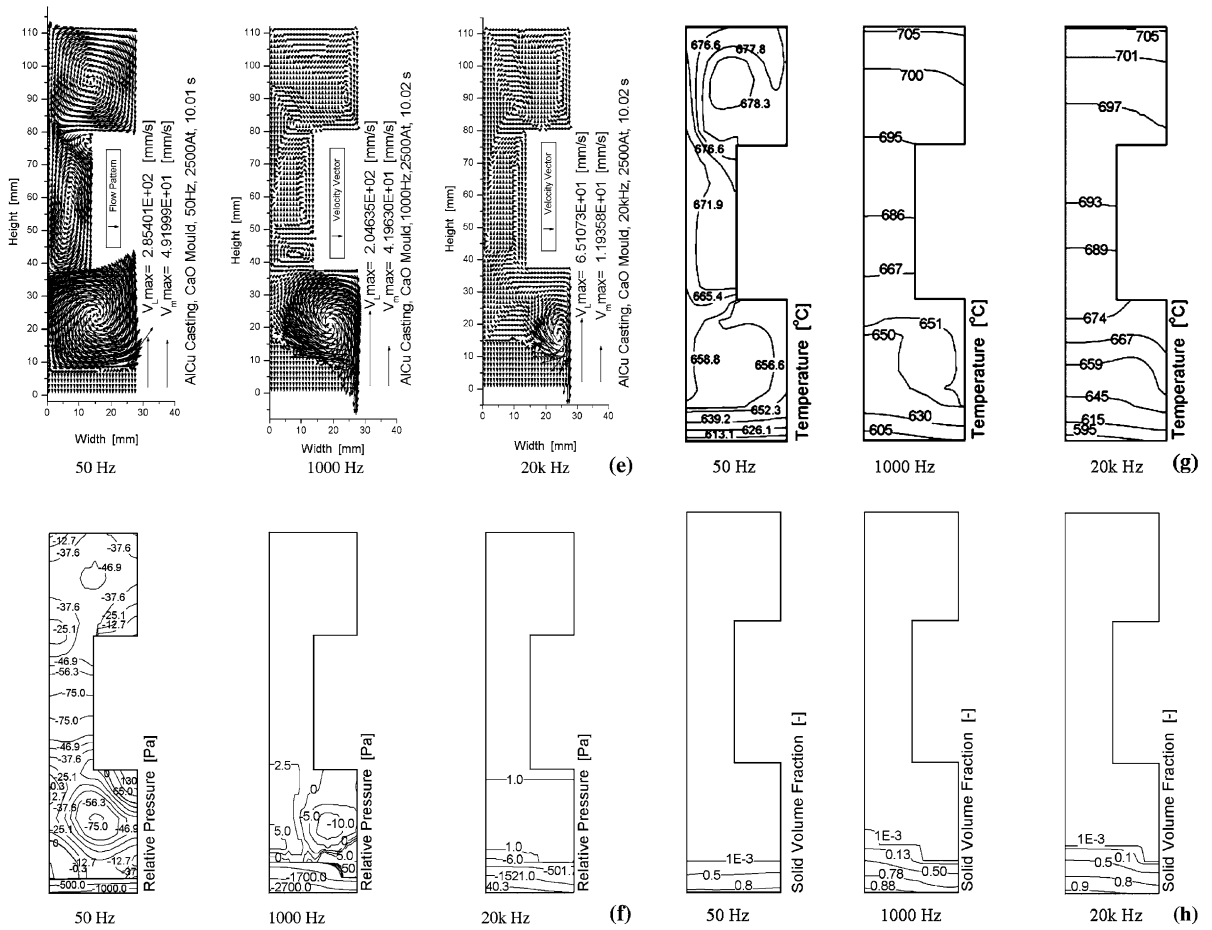

Fig. 5 (*continued*)

can be seen that for the case of 50 Hz, the much stronger EM-driven circulation causes the temperature distribution in the bulk liquid region to become uniform, and therefore results in the area of the directionally solidifying (S + L) region relatively smaller than the cases with the EM-frequencies of 1000 Hz and 20 kHz.

5. Conclusions

A previously modified continuum model [28,29] for describing the heat, mass and momentum transport phenomena in dendrite solidification processes of alloy castings/ingots was further extended to the solidification cases in a static or alternating electromagnetic field based on the theory of Thermo-Magneto Hydro Dynamics. Under the assumptions of small and negligible variations in the free-surface shape of the metallic melt during EM-solidification and constant/equal EM-properties of the solidifying materials, the couplings between the EM-fields and the STP-related fields can be simplified as one-way influences of the former on the STP behaviors in castings. In this case, full model solution to Eqs. (1)–(27) can be separated and use different numerical schemes.

Using the authors' proposed FDM-based numerical methods for STP solutions and a FEM-based commercial software for the EM-field analyses, the extended continuum model was successfully applied to the computer simulations of directional STP in blade-like castings of two different alloys under static or harmonic EM-fields. The computational results of the STP-behaviors in directionally solidifying In718 shaped castings under transverse static magnetic fields of different strengths reveal that, although the EMBR on the natural convections can be significantly effective, the volume-contraction-driven liquid feeding flow is much more difficult to be suppressed than the buoyancy-induced flow by means of applying a static magnetic field. On the other hand, an applied transverse static magnetic-field may promote the vertically parallel channel-segregations in a upwards directionally solidifying In718 casting to

form, because the homogenizing effects on the interdendritic solute redistributions by a liquid convection can be effectively weakened. The computational results on the EM-STP behaviors in directionally solidifying alloy shaped castings under alternating EM-fields of different frequencies demonstrate the availability of the present continuum modeling to reasonably account for the phenomenon of EM skin-effects in an EM-solidification process.

Acknowledgement

The authors wish to thank the supports for the present work from a Key China National Natural Science Foundation (NNSF) of grant no. 50395102 and a National Key Project of grant no. 41318.4.2.9.

References

[1] M.C. Flemings, in: Solidification Processing, McGraw-Hill Book Co., NY, 1974, pp. 224–258.
[2] W.D. Bennon, F.P. Incropera, A continuum model for momentum, heat and species transport in binary solid-liquid phase change system-I. model formulation, II. Application to solidification in a rectangular cavity, Int. J. Heat and Mass Transfer 30 (10) (1987) 2161–2170, pp. 2171–2187.
[3] C. Beckermann, R. Viskanta, Double-diffusive convection during dendritic solidification of a binary mixture, PCH PhysicoChemical Hydrodynam. 10 (2) (1988) 195–213.
[4] V.R. Voller, A.D. Brent, C. Prakash, The modeling of heat, mass and solute transport in solidification systems, Int. J. Heat and Mass Transfer 32 (9) (1989) 1719–1731.
[5] D.M. Xu, Q.Ch. Li, Numerical method for solution of strongly coupled binary alloy solidification problems, Numer. Heat Transfer, Part A 20 (1991) 181–201.
[6] D.M. Xu, Q.Ch. Li, Gravity- and solidification-shrinkage-induced liquid flow in a horizontally solidified alloy ingot, Numer. Heat Transfer, Part A 20 (1991) 203–221.
[7] H. Shahani, G. Amberg, H. Fredriksson, On the formation of macrosegregations in unidirectionally solidified Sn–Pb and Pb–Sn alloys, Metall. Trans. A 23A (1992) 2301–2311.
[8] J. Ni, C. Beckermann, A volume-averaged two-phase model for transport phenomena during solidification, Metall. Trans B 22B (1991) 349–361.
[9] C.Y. Wang, C. Beckermann, Equiaxed dendritic solidification with convection: part I. Multiscale/multiphase modeling, Metall. Mater. Trans. A 27A (1996) 2754–2764.
[10] C.Y. Wang, C. Beckermann, Equiaxed dendritic solidification with convection: part II. numerical simulations for an Al–4 wt%Cu alloy, Metall. Mater. Trans. A 27A (1996) 2765–2783.
[11] K.C. Chiang, H.L. Tsai, Interaction between shrinkage-induced fluid flow and natural convection during alloy solidification, Int. J. Heat and Mass Transfer 35 (7) (1992) 1771–1778.
[12] S. Chang, D.M. Stefanescu, A model for macrosegregation and its application to Al–Cu castings, Metall. Mater. Trans. A 27A (1996) 2708–2721.
[13] M.C. Flemings, G.E. Nereo, Macrosegregation: part III, Trans. Metall. Soc. AIME 242 (1968) 50–55.
[14] D.M. Xu, X.J. Wang, Q.Ch. Li, R.D. Pehlke, Control of dendrite structure and macrose gregation in directionally solidified castings with section variations, AFS Trans. 101 (1997) 861–868.
[15] S. Asai, Recent development and prospect of electromagnetic processing of materials, Sci. Technol. Adv. Mater. 1 (2000) 191–200.
[16] S. Kaddeche, D. Henry, T. Putelat, H. Ben Hadid, Instabilities in liquid metals controlled by constant magnetic field—part I: vertical magnetic field, J. Crystal Growth 242 (2002) 491–500.
[17] S. Kaddeche, H. Ben Hadid, T. Putelat, D. Henry, Instabilities in liquid metals controlled by constant magnetic field—part II: horizontal magnetic field, J. Crystal Growth 242 (2002) 501–510.
[18] K. Kakimoto, H. Ozoe, Oxygen distribution at a solid-liquid interface of silicon under transverse magnetic fields, J. Crystal Growth 212 (2000) 429–437.
[19] N.G. Ivanov, A.B. Korsakov, E.M. Smirnov, K.V. Khodosevitch, V.V. Kalaev, Yu.N. Makarov, E. Dornberger, J. Virbulis, W. von Ammon, Analysis of magnetic field effect on 3-D melt flow in CZ Si growth, J. Crystal Growth 250 (2003) 183–188.
[20] K. Takatani, K. Nakai, N. Kasai, T. Watanabe, H. Nakajima, Analysis of heat transfer and fluid flow in the continuous casting mold with electromagnetic brake, ISIJ Int. 29 (12) (1989) 1063–1068.
[21] H.L. Yang, X.Zh. Zhang, Sh.T. Qi, K.W. Deng, W.C. Li, Y. Gan, Mathematical study on EMBR in a slab continuous casting process, Scand. J. Metall. 27 (1998) 196–204.
[22] E. Takeuchi, Applying MHD technology to the continuous casting of steel slab, J. Metals (JOM) (May) (1995) 42–45.
[23] J.W. Evans, The use of electromagnetic casting for Al alloys and other metals, J. Metals (JOM) (May) (1995) 38–41.
[24] J. Sakane, B.Q. Li, J.W. Evans, Mathematical modeling of meniscus profile and melt flow in electromagnetic casters, Metall. Trans. B 19B (1988) 397–408.
[25] T. Li, S. Nagaya, K. Sassa, S. Asai, Study of meniscus behavior and surface properties during casting in a high-frequency magnetic field, Metall. Mater. Trans. B 26B (1995) 353–359.
[26] Ch. Vivès, Electromagnetic refining of aluminum alloys by the CREM process: part I. working principle and metallurgical results, Metall. Trans. B 20B (1989) 623–629.
[27] Ch. Vivès, Effects of forced electromagnetic vibrations during the solidification of aluminum alloys: part II. solidification in the presence of colinear variable and stationary magnetic fields, Metall. Mater. Trans. B 27B (1996) 457–464.
[28] D.M. Xu, A unified micro-scale parameter approach to solidification-transport phenomena-based macrosegregation modeling for dendritic solidification: part I. mixture average based analysis, Metall. Mater. Trans. B 32B (2001) 1129–1141.

[29] D.M. Xu, A unified micro-scale parameter approach to solidification-transport process-based macrosegregation modeling for dendritic solidification: part II. Numerical example computations, Metall. Mater. Trans. B 33B (2002) 451–463.
[30] D.M. Xu, J.J. Guo, H.Zh. Fu, W.Sh. Bi, Influences of dendrite morphologies and solid-back diffusion on macrosegregation in directionally solidified blade-like casting, Mater. Sci. Eng. A 344 (1–2) (2003) 64–73.
[31] T. Tanahashi, Theory and application of thermo-magneto hydro dynamics (I); (II) and (III), Tetsu-to-Hagane 79 (2, 4 & 5) (1993) N91–N102, N263–N281; N327–N342.
[32] X. Tong, C. Beckermann, A. Karma, Phase-field simulation of dendritic crystal growth in a forced flow, Phys. Rev. E 63 (2001) 1–16.
[33] D.M. Xu, J.J. Guo, H.Zh. Fu, Y.Q. Su, Q.Ch. Li, Numerical solution to T–φ_S–C_L coupling in binary dendrite solidification with any solid-back diffusion effects, Trans. Nonferrous Metals Soc. China 13 (5) (2003) 1149–1154.
[34] D.M. Xu, Y.F. Bai, J.J. Guo, H.Zh. Fu, Numerical simulation of heat, mass and momentum transport behaviors in directionally solidifying alloy castings under electromagnetic fields using an extended direct-SIMPLE scheme, Int. J. Numer. Methods Fluids 46 (2004) 767–791.
[35] Y.F. Bai, D.M. Xu, L.H. Mao, J.J. Guo, H.Zh. Fu, FEM/FDM-joint simulation for transport phenomena in directional solidifying shaped TiAl casting under electromagnetic field, ISIJ Int. 44 (7) (2004) 1173–1179.
[36] L.H. Mao, Computer simulation of transport phenomena in directionally solidified titanium alloy blade casting under electromagnetic fields, Master thesis, Harbin Institute of Technology, Harbin, 2003.
[37] L. Nastac, D.M. Stefanescu, Macrotransport-solidification kinetics modeling of equiaxed dendritic growth: part II. Computation problems and validation on INCONEL 718 superalloy castings, Metall. Mater. Trans. A 27A (1996) 4075–4083.
[38] D.M. Xu, G.Y. An, Computer simulation studies on precision casting technology and solidification transport processes of titanium alloys including TiAl, an Internal Research Report, Harbin Institute of Technology, Harbin, March 2000.
[39] I. Ohnaka, M. Matsumoto, Computer simulation of macrosegregation in ingots, Tetsu-to-Hagane 73 (1987) 1698–1705.